This article has been accepted for publication in a future issue of this journal, but has not been fully edited. Content may change prior to final publication. Citation information: DOI 10.1109/TSG.2021.3099206, IEEE Transactions on Smart Grid

Integrating Battery Aging in the Optimization for Bidirectional Charging of Electric Vehicles

Karl Schwenk, *Student Member, IEEE,* Stefan Meisenbacher, Benjamin Briegel, Tim Harr, Veit Hagenmeyer, *Member, IEEE,* and Ralf Mikut.

***Abstract*—Smart charging of Electric Vehicles (EVs) reduces operating cost, allows more sustainable battery usage, and promotes the rise of electric mobility. In addition, bidirectional charging and improved connectivity enable efficient power grid support. Today, however, uncoordinated charging, e.g. governed by users' habits, is still the norm. Thus, the impact of upcoming smart charging applications is mostly unexplored. We aim to estimate the expenses inherent with smart charging, e.g. battery aging costs, and give suggestions for further research. Using typical onboard sensor data we concisely model and validate an EV battery. We then integrate the battery model into a realistic smart charging use case and compare it with measurements of real EV charging. The results show that i) the temperature dependence of battery aging calls for precise thermal models for charging power greater than 7 kW, ii) disregarding battery aging underestimates EVs' operating cost by approx. 30%, and iii) the profitability of Vehicle-to-Grid (V2G) services based on bidirectional power flow, e.g. *energy arbitrage*, depends on battery aging costs and the electricity price spread.**

***Index Terms*—Electric Vehicle Charging, Artificial Neural Network (ANN), Vehicle-to-Grid, Optimization, Smart Charging, Electric Vehicles, Energy Arbitrage**

NOTATION

- $\hat{x}$ indicates an estimate of x
- $\underline{x}$ and $\overline{x}$ indicate the lower and upper bounds of x
- x_n indicates the value of x at time t_n
- $\boldsymbol{x}_\mathrm{d}$ represents a discrete space between $\underline{x}$ and $\overline{x}$ for DDP

Parameters

e_nom	Nominal available battery capacity (kWh)
H_EV	Total battery capacity loss, EV application (-)
Δt	Duration of discrete time interval (min)
V_EV	Total battery value loss, EV application (€)
ϵ	Electricity price (€/kWh)
ϵ_mean	Mean workday electricity price (€/kWh)
η	Efficiency of charging process (-)
λ	DDP penalty cost (€)

Variables

e	Battery energy (kWh)
e_max	Maximum available battery capacity (kWh)
ΔE	Energy throughput (kWh)
H	Battery state of health (-)
ΔH_cyc	Cyclic battery capacity loss (-)
ΔH_cal	Calendar battery capacity loss (-)
I_bat	Battery current (A)
$\boldsymbol{J}$	DDP cached total cost (€)
J_E	Energy cost function (€)
J_D	Battery degradation cost function (€)
$\mathfrak{J}$	DDP cost grid (€)
N	Number of time intervals (-)
$\mathcal{N}$	Set of time intervals (-)
p	Gross charging power (kW)
$\boldsymbol{p}^*$	Optimal charging power trajectory (kW)
$\mathfrak{P}$	DDP optimal action grid (kW)
$\dot{Q}_\mathrm{loss}$	Heat flow from internal battery losses (kW)
R_i	Battery internal resistance (Ω)
U_OCV	Battery open-circuit voltage (V)
U_bat	Battery terminal voltage (V)
γ	Electricity price spread (-)
θ	Battery temperature (°C)
$\Delta\Theta$	Battery temperature difference (K)
τ	Battery aging time equivalent (s)

Acronyms

ANN	Artificial Neural Network
DDP	Discrete Dynamic Programming
ECM	Equivalent Circuit Model
EV	Electric Vehicle
MAE	Mean Absolute Error
RMSE	Root Mean Squared Error
SC	Smart Charging
SOC	State of Charge
SOH	State of Health
V2G	Vehicle-to-Grid

Manuscript received 09/23/2020; revised 04/19/2021 and 07/01/2021; accepted 07/15/2021. The authors thank Mercedes-Benz AG (Sindelfingen, Germany) for the allocated resources and data required for this work. SM, RM and VH are funded by the Helmholtz Association under the Program Energy System Design and the Joint Initiative "Energy System 2050 – A Contribution of the Research Field Energy". K. Schwenk is with Mercedes-Benz AG, Sindelfingen, Germany, and the Institute for Automation and Applied Informatics, Karlsruhe Institute of Technology, Karlsruhe, Germany (e-mail: karl.schwenk@daimler.com; karl.schwenk@kit.edu). B. Briegel, and T. Harr are with Mercedes-Benz AG, Sindelfingen, Germany (e-mail: benjamin.briegel@daimler.com; tim.harr@daimler.com). S. Meisenbacher, V. Hagenmeyer and R. Mikut are with the Institute for Automation and Applied Informatics, Karlsruhe Institute of Technology, Karlsruhe, Germany (e-mail: stefan.meisenbacher@kit.edu; veit.hagenmeyer@kit.edu; ralf.mikut@kit.edu).

I. INTRODUCTION

UNDOUBTEDLY, Electric Vehicles (EVs) are on the rise. In this context, Smart Charging (SC), i.e. the controlled and coordinated charging of EVs, helps to minimize EV operating cost [18] and prolong EV battery life [2]. To further diminish negative power grid impacts due to EV charging,

This work is licensed under a Creative Commons Attribution 4.0 License. For more information, see https://creativecommons.org/licenses/by/4.0/

This article has been accepted for publication in a future issue of this journal, but has not been fully edited. Content may change prior to final publication. Citation information: DOI 10.1109/TSG.2021.3099206, IEEE Transactions on Smart Grid

TABLE I: Comparison of the proposed work with related works according to distinct technical features, see Sec. II.

References	A) EV User Perspective Adequately Represented	B) Battery Aging Considered as Monetary Costs	C) Optimization-based Smart Charging Application	D) Thermal Battery Model based on EV Sensor Data	E) Real-world Data for Modeling and Validation
[1]–[3]	✗	✗	✓	✗	✓
[4], [5]	✓	✓	✗	✗	✗
[6]–[13]	✓	✓	✓	✗	✗
[14]–[16]	✓	✓	✓	✗	✓
[17]	✗	✗	✗	✓	✓
proposed work	✓	✓	✓	✓	✓

Vehicle-to-Grid (V2G), which usually leverages bidirectional power flow, becomes important [19].[1]

Adoption of SC concepts, however, strongly depends on EV user acceptance [20]. Nowadays, EV users typically use manual charging in which the battery is fully charged at maximum available power after plugging in. For SC, EV users demand similar transparency in terms of operating cost [21]. SC applications usually consist of multi-dimensional decision problems with various objectives. Instead of simple heuristics whose behavior and effects are easily comprehensible for the EV user, these problems require model-based optimization methods for solving [16], [22]. For this purpose, suitable EV battery models must be developed and validated with real-world data [23]. Thus, EV operating cost can be correctly determined and the real-world impact of SC can be explored.

Aiming to fulfill the aforementioned requirements, we first create a battery model that can be used in production EVs. The battery model is then integrated into a realistic SC scheme. Based on validation with real-world data, we draw conclusions for future work on SC.

This paper is structured as follows: Section II reviews and discusses related work. All models and their connections are outlined in Section III. Section IV describes an exemplary SC use case. Based on this, Section V presents the validation of the single model components and optimization results. In Section VI we summarize the major findings and give an outlook on future work.

II. Related Work

To properly define the scope of the proposed work, we conducted a literature review yielding 30 relevant references. We classified those based on the following five features (see also Tab. I):

A) Diffusion of SC applications strongly depends on EV user acceptance. This requires adequate representation of EV operating cost, and/or inclusion of user comfort [20].

B) Battery aging is a crucial factor for SC economics that may not be neglected [6]–[8], [24]. In addition, EV users desire transparent EV operating cost, including costs inherent in battery aging [21].

C) SC applications usually consist of multi-dimensional and multi-objective decision problems that require advanced techniques for solving, e.g. model-based optimization [16], [22] or model-free reinforcement learning [9].

D) The battery temperature is an important factor for efficiency and battery aging [19], [25]. Therefore, a thermal battery model suitable for application with typical EVs sensor data is required.

E) The complexity of SC use cases, e.g. several stakeholders and financial value streams, calls for real-world data for both modeling and validation [23].

Out of the 30 references we further analyzed [1]–[17], as these possess at least two of the aforementioned features; a representative excerpt is given in the following.

Already in 2011 *Lunz et al.* [14] applied a genetic optimization algorithm to bidirectional charging of plug-in hybrid EVs. Considering dynamic energy tariffs and battery aging costs, EVs' operating cost was reduced compared with uncoordinated charging. However, a detailed battery model, e.g. including a thermal model, was not implemented.

Brinkel et al. [15] conducted a study on grid reinforcement with respect to limits of low voltage grid transformers and CO_2 emissions. The cost for EV charging was reduced by 13.2%. For the study, however, several EVs were aggregated and a simplified battery model was implemented.

Das et al. [16] set up an optimization-based SC scheme in a micro grid. The authors aimed to minimize energy costs, battery aging, and CO_2 emissions, while maximizing grid utilization. To adequately combine the perspectives of all stakeholders, the authors concluded that a multi-objective decision process is required. Although a 28.1% reduction of battery aging was reported for some cases, the applied battery model neither considered calendar aging nor the battery's thermal behavior.

Li et al. [2] used particle swarm optimization to design a SC scheme targeting minimal battery aging and grid load fluctuations. To quantify battery aging, a novel rain-flow cycle counting algorithm was used. The approach, however, inadequately represents the EV user perspective, as both variable electricity tariffs and monetary battery aging costs were neglected.

In [17], *Petit et al.* set up a SC application using an empirical battery aging model that considers electro-thermal influences. The case study for validation, however, was based on a heuristic that neglects important factors from an EV user perspective, e.g. energy and battery aging costs.

To the best of the authors' knowledge, none of the related works found in the literature considers all five features as indicated in Tab. I. Hence, we summarize the contributions of this paper as follows:

[1]Note that in this work we consider V2G as a derivative of SC.

This work is licensed under a Creative Commons Attribution 4.0 License. For more information, see https://creativecommons.org/licenses/by/4.0/

This article has been accepted for publication in a future issue of this journal, but has not been fully edited. Content may change prior to final publication. Citation information: DOI 10.1109/TSG.2021.3099206, IEEE Transactions on Smart Grid

- We use data of real-world charging events to design and validate a vehicle-specific battery model; this comprises the battery's electrical, thermal, and aging behavior. All models can be operated with inputs from typical onboard sensors in production EVs.
- This battery model is integrated in an optimization-based SC scheme. We then use Discrete Dynamic Programming (DDP) as a robust solving method. For validation, we utilize data from real-world charging events and historical electricity market prices.
- To support future work on SC, we derive application-dependent suggestions on i) the necessity of thermal battery models, ii) the significance of battery aging costs, and iii) suitable electricity tariffs for profitable V2G applications.

III. Models of a Smart Charging Scheme

First, we introduce the notation for a charging event starting at arrival time t_0 and ending at departure time t_N.[2] The time horizon $[t_0, t_N]$ is divided into N time intervals of duration Δt and $N+1$ states. Accordingly, we define the set of intervals

$$\mathcal{N} = [0, N-1] \subset \mathbb{N}. \tag{1}$$

Each time interval $n \in \mathcal{N}$ starts at time t_n and ends at time t_{n+1}. Each battery state at $t_n \in [t_0, t_N]$ is characterized by the battery energy e_n, normalized as State of Charge (SOC), and the battery temperature θ_n. The charging power p_n is assumed to remain constant throughout a single time interval n.[3]

To represent the battery's charging behavior, we implement an electrical, thermal, and aging model, see Fig. 1a.[4] We refer to the combination of these three models as the battery model. The prospective use of this battery model in production EVs limits the model inputs to typical onboard sensor data. Further, an optimization scheme as shown in Fig. 1b serves to calculate an optimal charging power trajectory $\boldsymbol{p}^*$ for a single charging event.

A. Electrical Model

The energy level of the EV battery—and thus the SOC—changes with surrounding influences, especially the charging power p_n. An electrical battery model, see Fig. 1a, helps to calculate the battery energy trajectory. For this purpose, the energy throughput of the battery

$$\Delta E_n = e_{n+1} - e_n, \forall n \in \mathcal{N}, \tag{2}$$

is estimated for a given time interval n, battery temperature θ_n, battery energy e_n, battery's terminal voltage $U_{\text{bat},n}$, and charging power p_n.

We abstract the EV battery with an Equivalent Circuit Model (ECM) consisting of a voltage source U_{OCV} serially connected with the internal resistance R_{i}, see Fig. 2.[5] Due to the low dynamics of EV charging, more complex models, e.g. resistor-capacitor-pairs or electro-chemical models, are not required [26].

Both $U_{\text{OCV},n}$ and $R_{\text{i},n}$ depend on the battery temperature θ_n and the battery energy e_n; we assume their values to be constant throughout a single time interval n. We obtain R_{i} from a look-up table and use the measured terminal voltage $U_{\text{bat},n}$ to obtain the open-circuit voltage of the battery

$$U_{\text{OCV},n} = U_{\text{bat},n} - R_{\text{i},n} \cdot I_{\text{bat},n}, \tag{3}$$

with the battery current $I_{\text{bat}} > 0$ during charging, $U_{\text{bat}} > U_{\text{OCV}}$ for charging and $U_{\text{bat}} < U_{\text{OCV}}$ for discharging. Substituting the terminal voltage with

$$U_{\text{bat},n} = \frac{p_n}{I_{\text{bat},n}}, \tag{4}$$

and solving (3), we obtain the battery current[6]

$$I_{\text{bat},n} = \frac{-U_{\text{OCV},n} + \sqrt{U_{\text{OCV},n}^2 + 4R_{\text{i},n} \cdot p_n}}{2R_{\text{i},n}}. \tag{5}$$

The Ohmic [27] losses within the battery amount to

$$\dot{Q}_{\text{loss},n} = R_{\text{i},n} \cdot I_{\text{bat},n}^2. \tag{6}$$

Given the charging power p_n, we obtain the energy throughput

$$\Delta E_n = \Delta t \cdot \left(p_n - \dot{Q}_{\text{loss},n}\right). \tag{7}$$

Note that $\dot{Q}_{\text{loss},n} > 0$ occurs both while charging and discharging. Hence, it decreases $|\Delta E_n|$ during charging and increases $|\Delta E_n|$ during discharging.

B. Thermal Model

Both the internal battery parameters and battery aging depend on the battery temperature. Therefore, a thermal battery model, as shown in Fig. 1a, estimates the change in battery temperature

$$\Delta\Theta_n = \theta_{n+1} - \theta_n, \tag{8}$$

for a given time interval n, battery temperature θ_n, battery energy e_n, and charging power p_n.[7] As the thermal behavior of EV batteries follows complex, non-linear processes, e.g. electro-chemical heat sources or sinks, we use a data-driven modeling approach.

First, we explore time series data from real charging events of batteries installed and operated in EVs; we discretize this data with $\Delta t = 5$ min to obtain single training samples for each time step. Based on the Spearman [28] correlation coefficient, we screen out irrelevant features. We then perform mean and variance normalization to ensure a proper model training. The available training data underrepresents discharging, i.e. $p_n < 0$. However, as experiments with the installed battery show similar $R_{\text{i},n}$ for charging and discharging, we consider it acceptable to use absolute values for p_n and $I_{\text{bat},n}$.

For the machine learning models, we compare a linear regression model and different Artificial Neural Network

[2]The term "charging event" refers to the entire time window between arrival and departure of an EV at a charging station.

[3]Note that p_n represents the gross charging power consumed from the charging station without conversion losses.

[4]These models can be vehicle-, vehicle-type-, or battery-specific, thus limiting a generic reuse. General initialization followed by incremental adaption, however, is conceivable.

[5]This model represents dedicated power electronics, hence it is vehicle-specific.

[6]Despite two possible solutions only the greater one is physically feasible.

[7]Due to heat exchange with surrounding components, thermal battery models are mostly vehicle-type-specific.

This work is licensed under a Creative Commons Attribution 4.0 License. For more information, see https://creativecommons.org/licenses/by/4.0/

This article has been accepted for publication in a future issue of this journal, but has not been fully edited. Content may change prior to final publication. Citation information: DOI 10.1109/TSG.2021.3099206, IEEE Transactions on Smart Grid

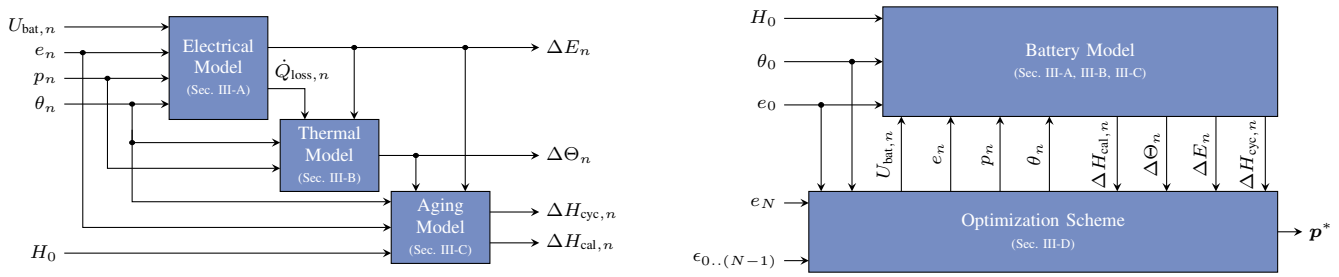

(a) Battery model and its components

(b) Optimization scheme for smart charging

Fig. 1: Layout of used models for smart charging application; battery model (Sec. III-A, III-B, III-C) (a); optimization scheme (Sec. III-D) (b).

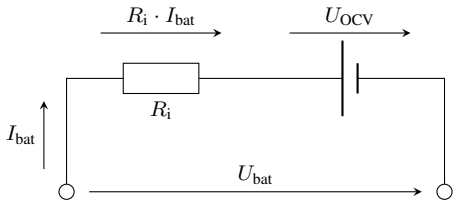

Fig. 2: Equivalent circuit model of an EV battery for low-dynamic operation with internal resistance R_i and voltage source U_OCV.

(ANN) models (multi layer perceptron with sigmoid activation function, learning rate of 0.001). As the optimal ANN model architecture (number of hidden layers, number of neurons per hidden layer) may vary for different input features, we use *grid-search* [29] to obtain the best performing model architecture. Applying a five-fold cross validation, we select the features

$$\{p_n, \dot{Q}_{\text{loss},n}, \Delta E_n, \theta_n\}, \tag{9}$$

to estimate $\Delta\Theta_n$. Note that we engineer the additional feature $\dot{Q}_{\text{loss},n}$ calculated in (6) based on domain knowledge. Hence, we uncover hidden relations for the machine learning algorithm (*gray-box* approach). We implement all models in *Python* [30] using *SciKit-Learn* [29] for linear regression and *Keras* [31] for ANNs.

C. Battery Aging Model

Irreversible physical and electro-chemical degradation processes (*battery aging*) cause the EV's usable driving range and monetary value to decrease. To quantify battery aging, the State of Health (SOH)

$$H = \frac{e_\text{max}}{e_\text{nom}} \leq 1, \tag{10}$$

indicates the maximum available storage capacity e_max compared with the nominal storage capacity e_nom. Calculating the evolution of e_max requires a battery aging model as described in the following.[8]

[8]Note that this model represents battery-specific aging characteristics that may differ for different types of battery cells; the proposed framework allows to accordingly replace the aging model, e.g. with models as in [32].

Charging and discharging causes the battery's anode and cathode to decay (*cyclic aging*). Among other processes, a loss of active lithium material occurs due to mechanical stress, see also [33]; For the battery cells used in this study, the cyclic aging increment

$$\Delta H_{\text{cyc},n} = \beta_\text{A} \cdot |\Delta E_n|^{\beta_\text{B}}, \tag{11}$$

only depends on the absolute energy throughput ΔE_n.

Additionally, high battery temperature and SOC cause degradation of both active and inactive battery components, see also [33]. Hence, the battery capacity fades over time, regardless of the energy throughput (*calendar aging*). For the battery cells used in this work, we describe the calendar aging increment

$$\Delta H_{\text{cal},n} = \tag{12}$$
$$1 - H_0 + \beta_\text{C} \exp\left(\frac{\beta_\text{D}}{273 + \theta_n} + \beta_\text{E} e_n\right) \cdot (\Delta t + \tau_n)^{\beta_\text{F}},$$

based on ARRHENIUS [34] curves. Here, H_0 is the SOH at the beginning of the charging event.[9] Furthermore,

$$\tau_n = \left(\frac{H_0 - 1}{\beta_\text{C} \exp\left(\frac{\beta_\text{D}}{273+\theta_n} + \beta_\text{E} e_n\right)}\right)^{1/\beta_\text{F}}, \tag{13}$$

represents the equivalent battery age for each time interval $n \in \mathcal{N}$ as a function of H_0.

Both model characteristics and parameters are estimated from extensive cell tests at varying conditions, e.g. battery energy and temperature. Hence, the detailed parameters $\beta_{\text{A..F}}$ depend on battery (cell) type and are confidential. Prospectively, an implicit representation, e.g. via machine learning approaches as in [35] is conceivable.

D. Optimization Scheme

Calculating a charging event's power trajectory requires appropriate algorithms, e.g. optimization-based SC schedul-

[9]H_0 serves as a reference for all time steps of one charging event, as calendar aging occurs on larger time scales (years) than charging (hours).

This work is licensed under a Creative Commons Attribution 4.0 License. For more information, see https://creativecommons.org/licenses/by/4.0/

This article has been accepted for publication in a future issue of this journal, but has not been fully edited. Content may change prior to final publication. Citation information: DOI 10.1109/TSG.2021.3099206, IEEE Transactions on Smart Grid

ing schemes. We therefore modify the vehicle- and battery-independent optimization scheme from [16] to be

$$\min_{\boldsymbol{p}\in\mathbb{R}^N} \sum_{\forall n\in\mathcal{N}} J_{\mathrm{E},n}(p_n,\epsilon_n) + J_{\mathrm{D},n}(\theta_n, e_n, H_0) \tag{14a}$$

subject to

$$\underline{\boldsymbol{p}} \le \boldsymbol{p} \le \overline{\boldsymbol{p}}, \quad \boldsymbol{p}\in\mathbb{R}^N, \tag{14b}$$
$$\underline{\boldsymbol{e}} \le \boldsymbol{e} \le \overline{\boldsymbol{e}}, \quad \boldsymbol{e}\in\mathbb{R}^{N+1}, \tag{14c}$$
$$\underline{e}_0 = e_0 = \overline{e}_0, \tag{14d}$$
$$\underline{e}_N = e_N = \overline{e}_N, \tag{14e}$$
$$\underline{\boldsymbol{\theta}} \le \boldsymbol{\theta} \le \overline{\boldsymbol{\theta}}, \quad \boldsymbol{\theta}\in\mathbb{R}^{N+1}, \tag{14f}$$
$$\underline{\theta}_0 = \theta_0 = \overline{\theta}_0, \tag{14g}$$
$$e_{n+1} = e_n + \Delta E\left(e_n, \theta_n, p_n\right), \quad \forall n\in\mathcal{N}, \tag{14h}$$
$$\theta_{n+1} = \theta_n + \Delta\Theta\left(e_n, p_n\right), \quad \forall n\in\mathcal{N}. \tag{14i}$$

Figure 1b shows the interaction of the optimization scheme and the proposed battery model. The components (14a)-(14i) and the solving method are described in the following.

1) Cost Functions: The optimization objective (14a) is to minimize the sum of energy costs $J_{\mathrm{E},n}$ and aging costs $J_{\mathrm{D},n}$ over all time intervals $n\in\mathcal{N}$.

To consider the costs for charging electric energy, we define the energy cost function

$$J_{\mathrm{E},n} = \begin{cases} J^{+}_{\mathrm{E},n}, & \forall p_n \ge 0, \\ J^{-}_{\mathrm{E},n}, & \forall p_n < 0, \end{cases} \tag{15}$$

with the energy expenses $J^{+}_{\mathrm{E},n} = p_n\cdot\Delta t\cdot\epsilon_n$, and the energy rewards $J^{-}_{\mathrm{E},n} = p_n\cdot\Delta t\cdot\epsilon_n$. For $p_n \ge 0$, the EV battery is charged at the electricity price ϵ_n. With $p_n < 0$, ϵ_n corresponds to the price of selling energy back to the grid; ϵ_n is given and assumed to be deterministic.

Battery aging also contributes to the total operating cost, as the EV's monetary value depends on the maximum usable battery capacity $e_{\max}$. Based on $\Delta H_{\mathrm{cyc},n}$ and $\Delta H_{\mathrm{cal},n}$ (Sec. III-C) we define the battery aging costs

$$J_{\mathrm{D},n} = \underbrace{\Delta H_{\mathrm{cyc},n}\cdot\frac{V_{\mathrm{EV}}}{H_{\mathrm{EV}}}}_{J^{\mathrm{cyc}}_{\mathrm{D},n}} + \underbrace{\Delta H_{\mathrm{cal},n}\cdot\frac{V_{\mathrm{EV}}}{H_{\mathrm{EV}}}}_{J^{\mathrm{cal}}_{\mathrm{D},n}}, \tag{16}$$

with the cyclic aging costs $J^{\mathrm{cyc}}_{\mathrm{D},n}$ and the calendar aging costs $J^{\mathrm{cal}}_{\mathrm{D},n}$.[10] Here, V_{EV} denotes the battery value loss due to the capacity loss H_{EV} during the battery's automotive application (*first life*). In particular, V_{EV} is the difference between the battery's production price and its residual value in a *second life* market. Note that (16) only accounts for aging caused throughout the charging event. To include battery aging for trips in between charging events in future work, a superordinate scheme as in [36] could determine the optimal target energy e_N.

[10]Given the non-linearity in (11) and (12), (16) also introduces non-linearity to (14).

2) Decision Variable: To obtain the optimal charging power trajectory, we define the decision variable

$$\boldsymbol{p} = (p_0, p_1, ..., p_{N-1})^{\top} \in \mathbb{R}^N, \tag{17}$$

with the charging power p_n in all time intervals $n\in\mathcal{N}$. Evaluating (14b) component-wise represents the power limitations with the upper bounds $\overline{\boldsymbol{p}}$ and lower bounds $\underline{\boldsymbol{p}}$. We assume these bounds to be constant throughout a single charging event. Both $\overline{\boldsymbol{p}}$ and $\underline{\boldsymbol{p}}$ are known at the time of computation and predefined e.g. by grid load constraints, charging stations, or EV power electronics.

3) State Variables: To compute the SOC of the battery, we define the state variable

$$\boldsymbol{e} = (e_0, e_1, e_2, ..., e_N)^{\top} \in \mathbb{R}^{N+1}, \tag{18}$$

representing the battery energy trajectory throughout a charging event. Reading (14c) component-wise reveals the energy limitations $\overline{\boldsymbol{e}}$ and $\underline{\boldsymbol{e}}$ that are constant and known at the time of computation. Their values are determined by physical restrictions, i.e. battery capacity, and/or EV user preferences, e.g. a minimum SOC.[11] We specify e_0 as the battery energy at the beginning of the charging event in (14d). The desired battery energy at departure e_N is determined by the user in (14e); prospectively, a previous calculation of e_N as in [36] can also be used.

For the battery temperature we similarly define the state variable

$$\boldsymbol{\theta} = (\theta_0, \theta_1, \theta_2, ..., \theta_N)^{\top} \in \mathbb{R}^{N+1}. \tag{19}$$

The temperature limits $\overline{\boldsymbol{\theta}}$ and $\underline{\boldsymbol{\theta}}$ in (14f) restrict $\boldsymbol{\theta}$ to be within a safe operating window given by the battery management system. Both $\overline{\boldsymbol{\theta}}$ and $\underline{\boldsymbol{\theta}}$ are constant and known at the time of computation. Additionally, the battery temperature θ_0 at the beginning of the charging event is given in (14g).

4) Battery Dynamics: To represent the evolution of the battery energy e_n we formulate (14h). Specifically, the electrical model in Sec. III-A is used to calculate e_{n+1} for each time interval $n\in\mathcal{N}$ (see also Fig. 1b). In a similar manner, (14i) describes the battery's thermal behavior based on the thermal model in Sec. III-B.

5) Method of Solving: As the non-linear models in (14h)-(14i) increase the complexity of (14), we use DDP [37] for solving; the detailed solving Algorithms 1-3 are given in the appendix. First, Algorithm 1 initializes the cost grid $\mathfrak{J}$, spanned by $\boldsymbol{e}, \boldsymbol{\theta}$ and time intervals $n\in\mathcal{N}$. Then, Algorithm 2 runs backwards ($n = N..0, \forall n\in\mathcal{N}$) to update $\mathfrak{J}$ for all possible $e_i \in \boldsymbol{e}_{\mathrm{d}}$ and $\theta_j \in \boldsymbol{\theta}_{\mathrm{d}}$. Similarly, all corresponding optimal actions $\mathfrak{P}$ are determined (*backward induction*). To avoid infeasible trajectories, a penalty value λ is assigned to the according value in $\mathfrak{J}$, if a constraint (14b)-(14i) is violated. Finally, Algorithm 3 integrates forward in time ($n = 0..N, \forall n\in\mathcal{N}$), starting from the initial values e_0 and θ_0. For each $n\in\mathcal{N}$, the cost-optimal action is taken from $\mathfrak{P}$ based on the current state e_n and θ_n. This yields the globally optimal charging power trajectory $\boldsymbol{p}^*$ (*forward integration*) [37].

[11]Note that the use of an electrical model (Sec. III-A) in (14h) implicitly respects the battery's voltage constraints.

This work is licensed under a Creative Commons Attribution 4.0 License. For more information, see https://creativecommons.org/licenses/by/4.0/

This article has been accepted for publication in a future issue of this journal, but has not been fully edited. Content may change prior to final publication. Citation information: DOI 10.1109/TSG.2021.3099206, IEEE Transactions on Smart Grid

IV. Case Study

From ten real-world EVs equipped with cloud-connected data loggers, we obtain measured time series data of 279 unidirectional charging events covering a full year [38]; we discretize this data with $\Delta t = 5$ min. In each interval, we calculate ΔE and $\Delta\Theta$ with the battery models from Sec. III-A and III-B, and using the mean charging power, battery temperature and energy. Then, we determine the Root Mean Squared Error (RMSE) of actual and estimated ΔE and $\Delta\Theta$ for each time interval (*local error*). Furthermore, we quantify the error propagation when repeatedly applying the battery models (i.e. estimate ΔE and $\Delta\Theta$ based on estimations of previous time interval); we therefore calculate the Mean Absolute Error (MAE) of actual and estimated e_N and θ_N at the end of each charging event (*global error*).

To evaluate the optimization scheme (Sec. III-D), we select 45 real charging events that have sufficient duration ($t_N - t_0 \geq 2\,\mathrm{h}$) and set the parameters:

$$\underline{p} = -50\,\mathrm{kW} \quad \underline{e} = 8\ \mathrm{kWh} \quad \underline{\theta} = -25\,^\circ\mathrm{C} \quad H_{\mathrm{EV}} = 20\,\%$$
$$\overline{p} = 50\,\mathrm{kW} \quad e_{\mathrm{nom}} = e = 80\ \mathrm{kWh} \quad \overline{\theta} = 60\,^\circ\mathrm{C} \quad V_{\mathrm{EV}} = 6080\,€$$

In addition, the conditions of each charging event determine the values of $\underline{e}_0 = \overline{e}_0$ (battery energy at arrival), $\underline{e}_N = \overline{e}_N$ (battery energy at departure), and $\underline{\theta}_0 = \overline{\theta}_0$ (battery temperature at arrival). After solving (14) (see Sec. III-D5), we compare the operating cost in three modes:

- **Mode I:** No optimization, calculate energy and aging costs for measured energy and temperature profile.
- **Mode II:** Optimize for energy costs only, calculate aging costs afterward.
- **Mode III:** Optimize for both energy and aging costs.

We use historic hourly electricity market prices of 2018 for ϵ_n [39]. To attain a representative price level for private customers, we supplement typical fees (0.188 €/kWh) and taxes (19%). Then, we average the price curves over all workdays and weekends to level out price peaks due to electricity over- or underproduction. We thus obtain two characteristic hourly price tables for ϵ, see Fig. 3, to evaluate the average profitability of SC.

Note that the duration of each charging event represents deterministic EV user behavior; future work will also consider stochastic influences. Furthermore, $\boldsymbol{p}^*$ is calculated once at the beginning of each charging event; prospectively, an ongoing charging event may be adapted to dynamic changes, i.e. departure time, target energy e_N, or electricity tariff, via a user interface with a system as in [40].

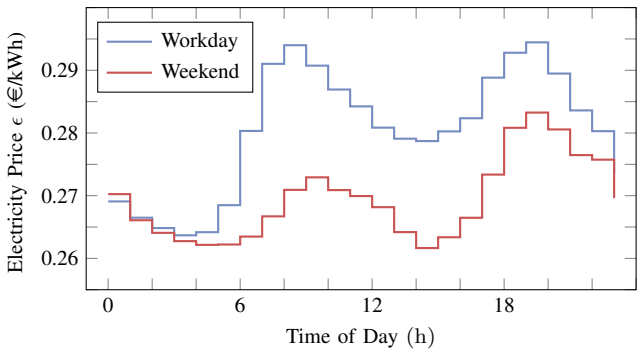

Fig. 3: Characteristic retail electricity price profiles ϵ for workdays and weekends supplemented by 0.188 €/kWh fees and 19% taxes [39].

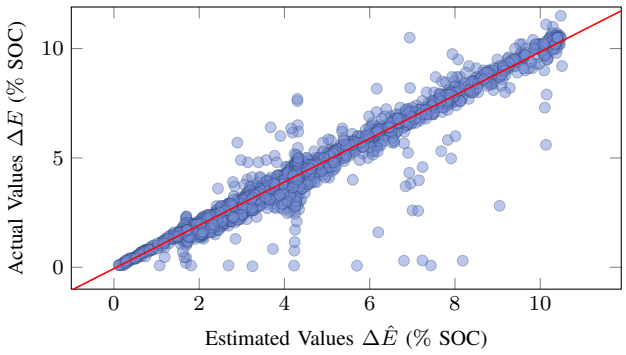

Fig. 4: Local error of electrical battery model (Sec. III-A), estimates per time interval $\Delta t = 5$ min; the red line indicates ideal model behavior.

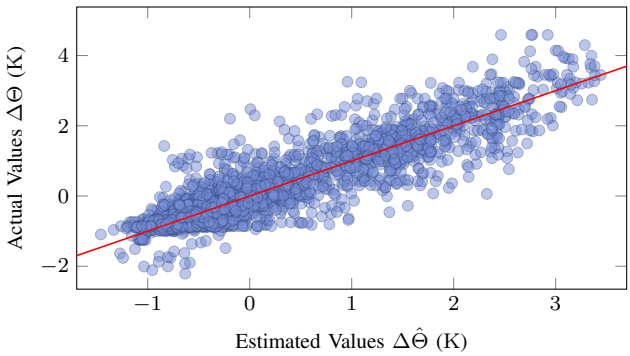

Fig. 5: Local error of best-performing data-driven thermal model (ANN, 2 hidden layers, 10 neurons each, Sec. III-B), estimates per time interval $\Delta t = 5$ min; the red line indicates ideal model behavior.

V. Results

A. Validation of the Battery Model

Table II presents the validation results of the battery model (Sec. III-A, III-B).

1) Validation of the Electrical Model: The electrical model (Sec. III-A) yields an RMSE of 0.35% SOC for single time intervals (local error, see Sec. IV). Hence, the model estimations $\Delta\hat{E}$ mostly match the actual values ΔE (Fig. 4). The model accuracy is improved, as both $U_{\mathrm{OCV},n}$ and $R_{\mathrm{i},n}$ are chosen from a look-up table for each time interval n depending on e_n and θ_n. Furthermore, high-dynamic changes of the battery energy are leveled out, as they occur on smaller time scales than the chosen $\Delta t = 5$ min [26]. When charging the battery to e_{max}, the battery management system corrects the characteristic SOC curve towards the end of the charging event; hence, a few outliers occur, e.g. with $\Delta E \cong 0$.

At the end of all charging events, the mean SOC deviation $E_N - \hat{E}_N$ is 2.37% SOC (global error, see Tab. II). This equals an acceptable driving range deviation of approx. 7.6 km, as

This work is licensed under a Creative Commons Attribution 4.0 License. For more information, see https://creativecommons.org/licenses/by/4.0/

This article has been accepted for publication in a future issue of this journal, but has not been fully edited. Content may change prior to final publication. Citation information: DOI 10.1109/TSG.2021.3099206, IEEE Transactions on Smart Grid

EV user's daily driven distance (mostly below $50\,\mathrm{km}$) is well within the battery range of $400\,\mathrm{km}$ [21]. We thus consider the accuracy of the electrical model as sufficient and deem $\Delta t = 5$ min and the ECM to be suitable for our case study.

2) Validation of the Thermal Model: To benchmark the thermal battery model (Sec. III-B), we assume constant battery temperature, i.e. $\theta_n = \theta_0, \forall n \in \mathcal{N}$ and $\Delta\hat{\Theta}_n = 0.0, \forall n \in \mathcal{N}$. In comparison with real charging events, assuming constant battery temperature yields an RMSE of 0.72 K for single time intervals (local error, see Sec. IV) and an MAE of 7.57 K at the end of a charging event (global error), see Tab. II.

As this result emphasizes the need for appropriate modeling, we test different data-driven thermal models and hyperparameters, see Sec. III-B. A linear regression model also misrepresents the battery's thermal behavior (see Tab. II), e.g. due to hidden electro-chemical processes.

More advanced ANN models, however, can capture the apparent non-linearity.[12] Using a distinct test data set, the ANN thermal model yields an RMSE of 0.29 K for single time intervals (local error), see Fig. 5. The MAE at the end of a charging event is 1.96 K (global error), see Tab. II. For our case study we deem this accuracy as sufficient (see also Sec. V-C). Yet, the input features of the data-driven thermal model seem to lack further influences on the battery's thermal behavior. The input features could therefore be enhanced, e.g. by internal cell temperatures or ambient conditions (temperature, sun radiation, wind). Note that typical EV onboard data, however, does not yet provide this information.

B. Operating Cost Evaluation

Figure 6 shows the operating cost components for all three modes described in Sec. IV normalized against the operating cost of Mode I. On average, Mode III yields a 7.8% lower operating cost compared with Mode I; similar results can be found in the literature, e.g. 5.4% in [8] and 13.2% with simplifications in [15]. Although $\underline{p} < 0$ in (14b), i.e. discharging the EV battery is possible, no energy rewards J_{E}^{-} can be observed in Mode III. This implies that J_{E}^{-} does not compensate for round-trip energy losses (charging and discharging) and aging costs.

Disregarding battery aging underestimates the total operating cost in Mode I by 30.1% on average; in [6] an underestimation of up to 52% is reported. This becomes apparent when applying Mode II: the optimization scheme utilizes price differences throughout the charging events to generate energy rewards. Thus, the energy costs (15) decrease by 13.3% compared with Mode I. Calculating the battery aging costs (16) afterward, however, yields a 55.8% higher total operating cost. Repeatedly charging and discharging the battery increases the battery temperature θ and causes the calendar aging costs $J_{\mathrm{D}}^{\mathrm{cal}}$ to rise in Mode II. *Trippe et al.* [6] report an even more drastic result for this setup: 8% electricity costs reduction, but a threefold increase of battery aging costs. Hence, we conclude that especially for charging with the allocation of V2G services–in this case *energy arbitrage*– battery aging must not be neglected.

[12]For the sake of brevity we only report the best-performing ANN model (two hidden layers, ten neurons each, sigmoid activation function).

TABLE II: Local and global error of electrical and thermal battery models (Sec. III-A, III-B).

Model	Local Error (RMSE)	Global Error (MAE)
Electrical ECM	0.35% SOC	2.37% SOC
Constant Battery Temperature	0.72 K	7.57 K
Linear Regression Thermal Model	0.76 K	4.18 K
ANN Thermal Model	0.29 K	1.96 K

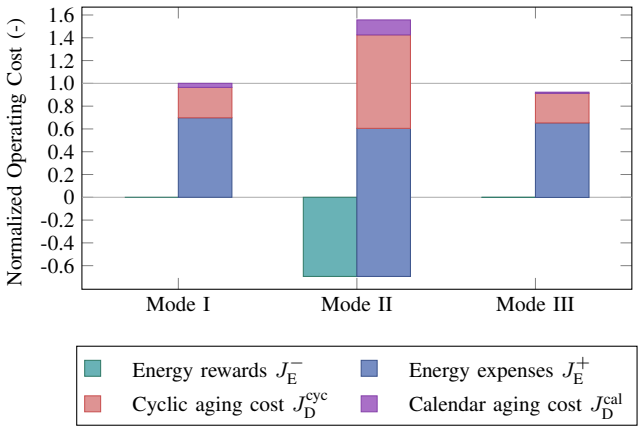

Fig. 6: Normalized operating cost and its components of 45 real charging events; Mode I (no optimization), Mode II (energy costs optimization), Mode III (energy and aging costs optimization).

C. Effects of Thermal Modeling

Including advanced thermal models, e.g. ANNs, increases the problem complexity and the computational effort to solve the resulting optimization problem. Therefore, we analyze the necessity of a thermal battery model as described in Sec. III-B. In Mode III, assuming constant battery temperature, i.e. $\Delta\Theta_n = 0.0, \forall n \in \mathcal{N}$, would underestimate the operating cost by 0.55% compared with a data-driven thermal model. Applying Mode II, however, the operating cost would be underestimated by 3.44%.

Besides the errors in estimating the operating cost, the presence of a thermal model also influences the decision made by the optimization scheme, i.e. the charging power trajectory $\boldsymbol{p}^*$. Figure 7 shows exemplary power profiles for i) assuming constant battery temperature and ii) using a data-driven thermal model. For $|p| > 7$ kW, the mean difference of charging power is 3.11 kW, when comparing the constant battery temperature assumption with the data-driven thermal model. However, for $|p| \leq 7$ kW the mean deviation of charging power only amounts to 0.75 kW.

Although the operating cost only show minor deviations, the charging power profiles change significantly. In particular, the relevance of the battery temperature rises with the (absolute) charging power. Hence, we suggest to use advanced thermal models, e.g. as in Sec. III-B for $|p| > 7$ kW. For $|p| \leq 7$ kW, assuming constant battery temperature suffices.

This work is licensed under a Creative Commons Attribution 4.0 License. For more information, see https://creativecommons.org/licenses/by/4.0/

This article has been accepted for publication in a future issue of this journal, but has not been fully edited. Content may change prior to final publication. Citation information: DOI 10.1109/TSG.2021.3099206, IEEE Transactions on Smart Grid

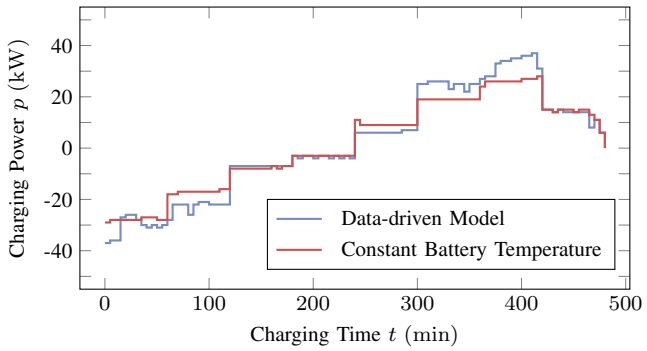

Fig. 7: Charging power profiles over time for constant battery temperature (red) and data-driven thermal model (blue, see also Sec. III-B).

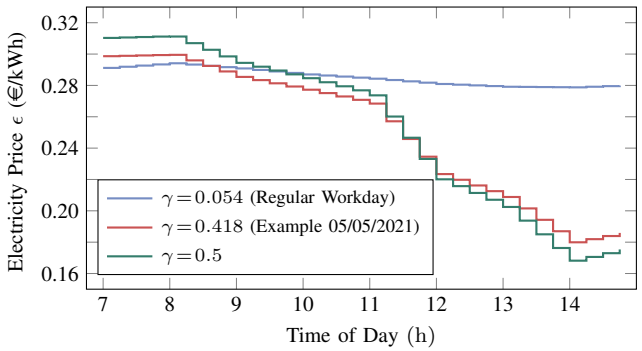

Fig. 8: Electricity price profiles with different spread γ [39].

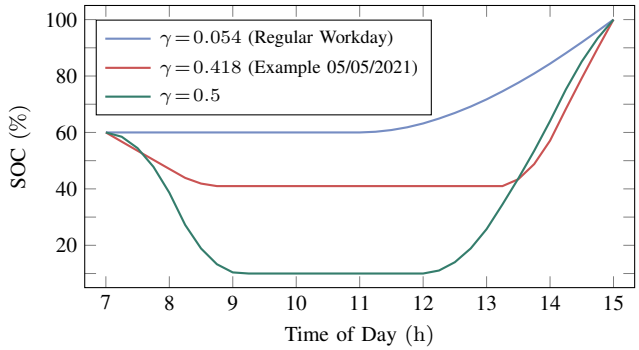

Fig. 9: SOC profiles over time for price profiles with different electricity spread factors γ, see Fig. 8.

D. Effects of Battery Prices

Due to EV market growth and battery technology improvements battery production prices will likely decrease within the next decade [41]–[43].[13] In anticipation of SC for EV fleets, we compare EV operating cost of real charging events (see Sec. IV) with future battery prices for 2025 ($V_{\mathrm{EV}} = 4470\,€$) and 2030 ($V_{\mathrm{EV}} = 2770\,€$) taken from [41].[14] This directly affects (16), i.e. the aging costs J_{D} could on average decrease by 26.5% in 2025 and by 54.4% in 2030 compared with 2020 battery prices ($V_{\mathrm{EV}} = 6080\,€$). Regarding the total operating cost, however, the decrease would only amount to 6.8% in 2025, or 15.9% in 2030, respectively. This reduction of battery aging costs is not sufficient for *energy arbitrage* to become profitable from a user's point of view. A conceivable setup for power suppliers to incentivize EV owners to participate in V2G services could be a flat compensation for battery aging costs per charging event.

E. Influence of Electricity Tariff

Using today's dynamic electricity tariffs (e.g. *aWATTar*[15]), V2G services such as *energy arbitrage* may be unprofitable (see Fig. 6). The reason could be insufficient price variations over time to compensate aging costs. To investigate, we quantify the spread of a charging event's price profile $\boldsymbol{\epsilon}$ as

$$\gamma = \frac{\max\{\boldsymbol{\epsilon}\} - \min\{\boldsymbol{\epsilon}\}}{\epsilon_{\mathrm{mean}}}, \tag{20}$$

with the mean workday price $\epsilon_{\mathrm{mean}} = 0.286\,€/\mathrm{kWh}$ as a reference. To evaluate the sensitivity of the optimization scheme to γ, we use an exemplary eight-hour charging event from 60% SOC to 100% SOC. Then, three price profiles with different γ are tested (Fig. 8). We first use a regular workday profile with $\gamma = 0.054$ (blue). Second, we analyze a real-world case from 2021 with slight electricity underproduction in the morning and overproduction in the afternoon ($\gamma = 0.418$, red).[16] Considering the rise of renewable energy sources in the future, such cases could occur more often [44]. Grid operators may then use EV batteries as power reserve to compensate drastic grid imbalances. Thus, a third, stretched profile of the real-world case with $\gamma = 0.5$ is used (green).

Figure 9 shows the resulting SOC profiles. For $\gamma = 0.054$ (blue), no discharging of the battery takes place. Instead, charging is delayed to reduce battery aging. In contrast, the SOC profile of the real-world case (Fig. 9, red) with $\gamma = 0.418$ shows discharging of the battery at the beginning, when ϵ is high. The battery is then maintained at a level of approx. 41% SOC and charged later, when ϵ is low. In this way, both energy costs are lowered (via *energy arbitrage*) and battery aging is reduced (by decreasing the charging event's mean SOC).

To guide future work on grid-supporting V2G services, we estimate a characteristic threshold for γ, see also [4], [45]. We assume discharging the battery in one time interval and charging in the second one with equal (absolute) power $|p| \leq 7$ kW. The characteristic threshold

$$\gamma^* = \frac{J_{\mathrm{E}} \cdot (1-\eta) + 2J_{\mathrm{D}}}{\epsilon_{\mathrm{mean}}}, \tag{21}$$

then represents the critical price spread above which V2G rewards fully compensate for battery aging and conversion losses. With $\theta = 21\,°\mathrm{C}$ and a round-trip energy efficiency $\eta = 0.997$, we obtain $\gamma^* = 0.431$. Thus, for this setting, V2G

[13] Also advances in battery technology, i.e. reduced battery aging, would have similar effects as decreasing battery production prices.

[14] To highlight the influence of decreasing battery prices, we assume 2018 electricity prices as the cost calculation's underlying future prices and use a setup as in Sec. IV.

[15] https://www.awattar.de/

[16] German day-ahead prices (05/05/2021), fees and taxes added [39].

This work is licensed under a Creative Commons Attribution 4.0 License. For more information, see https://creativecommons.org/licenses/by/4.0/

This article has been accepted for publication in a future issue of this journal, but has not been fully edited. Content may change prior to final publication. Citation information: DOI 10.1109/TSG.2021.3099206, IEEE Transactions on Smart Grid

potential is fully utilized if the price spread is above $43.1\,\%$ relative to $\epsilon_{\text{mean}} = 0.286\,€/\text{kWh}$. The green SOC profile in Fig. 9 with $\gamma = 0.5$ confirms this result. At the beginning, the battery is fully discharged to 10% SOC, i.e. the lower SOC bound, see (14c). After idling for approx. 3 h, the battery is charged to the target SOC of 100%. Accordingly, V2G is unprofitable for price profiles as in Fig. 3, where $\gamma = 0.107$ (workday) and $\gamma = 0.075$ (weekend) is significantly below γ^*.

Note that γ^* also depends on other quantities, e.g. a charging event's SOC and time range, whose influences need to be investigated in future work. The specific value of γ^* may thus not apply directly to other cases. Rather, a qualitative result can be concluded. Influencing EV charging processes externally (e.g. as grid operator) requires an adapted price policy. Instead of averaged price profiles (e.g. Fig. 8, blue), the fluctuations of the electricity market, such as extensive price peaks (Fig. 8, red), need to be passed to the EV customer.

VI. Conclusion

In the present work, we analyzed the influence of battery aging on Smart Charging (SC) of Electric Vehicles (EVs). We modeled the EV battery using onboard sensor data and set up an optimization-based SC use case. Evaluating the concept with real-world EV data revealed the need for advanced thermal models when charging power exceeds 7 kW. We found that exploiting time and energy flexibility of EV charging reduces operating cost by 7.8%. Furthermore, disregarding battery aging underestimates EVs' operating cost up to 30%. Battery aging costs thus hinders many Vehicle-to-Grid (V2G) services based on bidirectional power flow from being profitable. To overcome this would require a vast decrease of battery production prices or adapted electricity tariffs that directly represent market fluctuations. Future work will examine stochastic influences on SC. These comprise EV user behavior, random V2G service allocation, integration of renewable energy sources, and dynamic constraints of transformers and charging stations.

Appendix
Discrete Dynamic Programming Algorithms

Algorithm 1: Initialization of backward induction algorithm (see Algorithm 2), acc. [37].

Input: $N, e_0, e_N, \theta_0, \underline{e}, \overline{e}, \underline{\theta}, \overline{\theta}, \underline{p}, \overline{p}, \lambda$

 # discretize state and action:

$\boldsymbol{e}_\text{d} \leftarrow \texttt{range}(\text{start: } \underline{e}, \text{stop: } \overline{e}, \text{step: } 0.8 \text{ kWh})$

$\boldsymbol{\theta}_\text{d} \leftarrow \texttt{range}(\text{start: } \underline{\theta}, \text{stop: } \overline{\theta}, \text{step: } 1 \text{ K})$

$\boldsymbol{p}_\text{d} \leftarrow \texttt{range}(\text{start: } \underline{p}, \text{stop: } \overline{p}, \text{step: } 1 \text{ kW})$

 # initialize cost grid and action grid (penalty value $\lambda = 1000\,€$):

$\mathfrak{J} \leftarrow \texttt{zeros}(N, \texttt{length}(\boldsymbol{e}_\text{d}), \texttt{length}(\boldsymbol{\theta}_\text{d}))$

$\mathfrak{J}[0, :, :], \mathfrak{J}[N, :, :] \leftarrow \lambda, \lambda$

$\mathfrak{J}[0, \texttt{argmin}(|\boldsymbol{e}_\text{d} - e_0|), \texttt{argmin}(|\boldsymbol{\theta}_\text{d} - \theta_0|)] \leftarrow 0$

$\mathfrak{J}[N, \texttt{argmin}(|\boldsymbol{e}_\text{d} - e_N|), :] \leftarrow 0$

$\mathfrak{P} \leftarrow \texttt{zeros}(N, \texttt{length}(\boldsymbol{e}_\text{d}), \texttt{length}(\boldsymbol{\theta}_\text{d}))$

Output: $\mathfrak{J}, \mathfrak{P}, \boldsymbol{e}_\text{d}, \boldsymbol{\theta}_\text{d}, \boldsymbol{p}_\text{d}$

Algorithm 2: Backward induction algorithm to create cost grid $\mathfrak{J}$ and corresponding optimal actions $\mathfrak{P}$, acc. [37].

Input: $N, \mathfrak{J}, \mathfrak{P}, \boldsymbol{e}_\text{d}, \boldsymbol{\theta}_\text{d}, \boldsymbol{p}_\text{d}, \underline{e}, \overline{e}, \underline{\theta}, \overline{\theta}, \underline{p}, \overline{p}, \boldsymbol{\epsilon}, \lambda$

for $n \leftarrow N-1$ **to** 0 **:**

  for all $e_i \in \boldsymbol{e}_\text{d}$ **:**

    for all $\theta_j \in \boldsymbol{\theta}_\text{d}$ **:**

      # initialize cached total cost:

      $\boldsymbol{J} \leftarrow \texttt{ones}(\texttt{length}(\boldsymbol{p}_\text{d})) \cdot \lambda$

      for all $p_k \in \boldsymbol{p}_\text{d}$ **:**

        # validate charging power constraints (14b)*:*

        if $\underline{p}(e_i, \theta_j) \le p_k \le \overline{p}(e_i, \theta_j)$ **:**

          # calculate state transitions (Sec. III-A, III-B):

          $e_{n+1} \leftarrow e_i + \Delta E(e_i, \theta_j, p_k)$

          $\theta_{n+1} \leftarrow \theta_j + \Delta\Theta(p_k, \dot{Q}_\text{loss}(e_i, \theta_j, p_k), \Delta E(e_i, \theta_j, p_k), \theta_j)$

          # validate state constraints (14c) *and* (14f)*:*

          if $\underline{e} \le e_{n+1} \le \overline{e}$ **and** $\underline{\theta} \le \theta_{n+1} \le \overline{\theta}$ **:**

            # calculate transition costs (15) *and* (16)*:*

            $J_\text{E} \leftarrow J_\text{E}(p_k, \epsilon_n)$

            $J_\text{D} \leftarrow \frac{V_\text{EV}}{H_\text{EV}}(\Delta H_\text{cal}(e_i, \theta_j, H_0) + \Delta H_\text{cyc}(|\Delta E(e_i, \theta_j, p_k)|))$

            # calculate and cache total cost:

            $\boldsymbol{J}[k] \leftarrow J_\text{E} + J_\text{D} + \mathfrak{J}[\texttt{argmin}(|\boldsymbol{e}_\text{d} - e_{n+1}|), \texttt{argmin}(|\boldsymbol{\theta}_\text{d} - \theta_{n+1}|)]$

      # assign minimum cached cost and corresponding action:

      $\mathfrak{J}[n, i, j] \leftarrow \texttt{min}(\boldsymbol{J})$

      $\mathfrak{P}[n, i, j] \leftarrow \boldsymbol{p}_\text{d}[\texttt{argmin}(\boldsymbol{J})]$

Output: $\mathfrak{J}, \mathfrak{P}$

Algorithm 3: Forward integration algorithm to find the optimal charging power trajectory $\boldsymbol{p}^*$, acc. [37].

Input: $N, \mathfrak{J}, \mathfrak{P}, e_0, \theta_0, \boldsymbol{e}_\text{d}, \boldsymbol{\theta}_\text{d}, \boldsymbol{\epsilon}$

 # find starting point in the cost grid:

$i, j \leftarrow \texttt{argmin}(\mathfrak{J}[0, :, :])$

 # initialize output and assign corresponding action:

$\boldsymbol{p}^* \leftarrow \texttt{zeros}(N)$

$\boldsymbol{p}^*[0] \leftarrow \mathfrak{P}[0, i, j]$

 # initialize costs:

$J_\text{E}, J_\text{D} \leftarrow 0, 0$

 # start forward integration loop:

for $n \leftarrow 0$ **to** $N-1$ **:**

  # calculate state transitions (see Sec. III-A and III-B):

  $e_{n+1} \leftarrow e_n + \Delta E(e_n, \theta_n, \boldsymbol{p}^*[n])$

  $\theta_{n+1} \leftarrow \theta_n + \Delta\Theta(\boldsymbol{p}^*[n], \dot{Q}_\text{loss}(e_n, \theta_n, \boldsymbol{p}^*[n]), \Delta E(e_n, \theta_n, \boldsymbol{p}^*[n]), \theta_n)$

  # calculate costs with (15) *and* (16)*:*

  $J_\text{E} \leftarrow J_\text{E} + J_\text{E}(p_n, \epsilon_n)$

  $J_\text{D} \leftarrow J_\text{D} + \frac{V_\text{EV}}{H_\text{EV}}(\Delta H_\text{cal}(e_n, \theta_n, H_0)) + \Delta H_\text{cyc}(|\Delta E(e_n, \theta_n, \boldsymbol{p}^*[n])|)$

  # find nearest discrete state and assign corresponding action:

  $\boldsymbol{p}^*[n+1] \leftarrow \mathfrak{P}[n+1, \texttt{argmin}(|\boldsymbol{e}_\text{d} - e_{n+1}|), \texttt{argmin}(|\boldsymbol{\theta}_\text{d} - \theta_{n+1}|)]$

Output: $\boldsymbol{p}^*, J_\text{E}, J_\text{D}$

This work is licensed under a Creative Commons Attribution 4.0 License. For more information, see https://creativecommons.org/licenses/by/4.0/

This article has been accepted for publication in a future issue of this journal, but has not been fully edited. Content may change prior to final publication. Citation information: DOI 10.1109/TSG.2021.3099206, IEEE Transactions on Smart Grid

REFERENCES

[1] C. Crozier, T. Morstyn, M. Deakin, and M. McCulloch, "The case for bi-directional charging of electric vehicles in low voltage distribution networks," *Applied Energy*, vol. 259, p. 114214, 2020.

[2] S. Li, J. Li, C. Su, and Q. Yang, "Optimization of bi-directional v2g behavior with active battery anti-aging scheduling," *IEEE Access*, vol. 8, pp. 11 186–11 196, 2020.

[3] Q. Yang, J. Li, W. Cao, S. Li, J. Lin, D. Huo, and H. He, "An improved vehicle to the grid method with battery longevity management in a microgrid application," *Energy*, vol. 198, p. 117374, 2020.

[4] J. D. Bishop, C. J. Axon, D. Bonilla, and D. Banister, "Estimating the grid payments necessary to compensate additional costs to prospective electric vehicle owners who provide vehicle-to-grid ancillary services," *Energy*, vol. 94, pp. 715–727, 2016.

[5] T. Steffen, A. Fly, and W. Mitchell, "Optimal electric vehicle charging considering the effects of a financial incentive on battery ageing," *Energies*, vol. 13, no. 18, p. 4742, 2020.

[6] A. E. Trippe, R. Arunachala, T. Massier, A. Jossen, and T. Hamacher, "Charging optimization of battery electric vehicles including cycle battery aging," in *IEEE PES Innovative Smart Grid Technologies, Europe*. IEEE, 2014.

[7] H. Hesse, V. Kumtepeli, M. Schimpe, J. Reniers, D. Howey, A. Tripathi, Y. Wang, and A. Jossen, "Ageing and efficiency aware battery dispatch for arbitrage markets using mixed integer linear programming," *Energies*, vol. 12, no. 6, p. 999, 2019.

[8] Tayarani, Jahangir, Nadafianshahamabadi, Golkar, Ahmadian, and Elkamel, "Optimal charging of plug-in electric vehicle: Considering travel behavior uncertainties and battery degradation," *Applied Sciences*, vol. 9, no. 16, p. 3420, 2019.

[9] Z. Wan, H. Li, H. He, and D. Prokhorov, "Model-free real-time EV charging scheduling based on deep reinforcement learning," *IEEE Transactions on Smart Grid*, vol. 10, no. 5, pp. 5246–5257, 2019.

[10] M. Ebrahimi, M. Rastegar, M. Mohammadi, A. Palomino, and M. Parvania, "Stochastic charging optimization of v2g-capable PEVs: A comprehensive model for battery aging and customer service quality," *IEEE Transactions on Transportation Electrification*, vol. 6, no. 3, pp. 1026–1034, 2020.

[11] F. Grée, V. Laznikova, B. Kim, G. Garcia, T. Kigezi, and B. Gao, "Cloud-Based Big Data Platform for Vehicle-to-Grid (V2G)," *World Electric Vehicle Journal*, vol. 11, no. 2, p. 30, 2020.

[12] W. Vermeer, G. R. C. Mouli, and P. Bauer, "Real-Time Building Smart Charging System Based on PV Forecast and Li-Ion Battery Degradation," *Energies*, vol. 13, no. 13, p. 3415, 2020.

[13] K. Zhou, L. Cheng, X. Lu, and L. Wen, "Scheduling model of electric vehicles charging considering inconvenience and dynamic electricity prices," *Applied Energy*, vol. 276, p. 115455, 2020.

[14] B. Lunz, H. Walz, and D. U. Sauer, "Optimizing vehicle-to-grid charging strategies using genetic algorithms under the consideration of battery aging," in *2011 IEEE Vehicle Power and Propulsion Conference*. IEEE, 2011.

[15] N. B. G. Brinkel, W. L. Schram, T. A. AlSkaif, I. Lampropoulos, and W. G. J. H. M. van Sark, "Should we reinforce the grid? Cost and emission optimization of electric vehicle charging under different transformer limits," *Applied Energy*, vol. 276, p. 115285, 2020.

[16] R. Das, Y. Wang, G. Putrus, R. Kotter, M. Marzband, B. Herteleer, and J. Warmerdam, "Multi-objective techno-economic-environmental optimisation of electric vehicle for energy services," *Applied Energy*, vol. 257, p. 113965, 2020.

[17] M. Petit, E. Prada, and V. Sauvant-Moynot, "Development of an empirical aging model for li-ion batteries and application to assess the impact of vehicle-to-grid strategies on battery lifetime," *Applied Energy*, vol. 172, pp. 398–407, 2016.

[18] A. Schuller, B. Dietz, C. M. Flath, and C. Weinhardt, "Charging Strategies for Battery Electric Vehicles: Economic Benchmark and V2G Potential," *IEEE Transactions on Power Systems*, vol. 29, no. 5, pp. 2014–2022, 2014.

[19] G. Saldaña, J. I. S. Martin, I. Zamora, F. J. Asensio, and O. Oñederra, "Electric vehicle into the grid: Charging methodologies aimed at providing ancillary services considering battery degradation," *Energies*, vol. 12, no. 12, p. 2443, 2019.

[20] C. Will and A. Schuller, "Understanding user acceptance factors of electric vehicle smart charging," *Transportation Research Part C: Emerging Technologies*, vol. 71, pp. 198–214, 2016.

[21] Daimler AG, "Evaluation E-Mobility Concepts: Full Report," Internal Document, 2019.

[22] K. M. Tan, V. K. Ramachandaramurthy, and J. Y. Yong, "Integration of electric vehicles in smart grid: A review on vehicle to grid technologies and optimization techniques," *Renewable and Sustainable Energy Reviews*, vol. 53, pp. 720–732, 2016.

[23] R. Das, K. Thirugnanam, P. Kumar, R. Lavudiya, and M. Singh, "Mathematical modeling for economic evaluation of electric vehicle to smart grid interaction," *IEEE Transactions on Smart Grid*, vol. 5, no. 2, pp. 712–721, 2014.

[24] S. Nazari, F. Borrelli, and A. Stefanopoulou, "Electric vehicles for smart buildings: A survey on applications, energy management methods, and battery degradation," *Proceedings of the IEEE*, pp. 1–17, 2020.

[25] A. W. Thompson, "Economic implications of lithium ion battery degradation for Vehicle-to-Grid (V2X) services," *Journal of Power Sources*, vol. 396, pp. 691–709, 2018.

[26] G. Plett, "High-Performance Battery-Pack Power Estimation Using a Dynamic Cell Model," *IEEE Transactions on Vehicular Technology*, vol. 53, no. 5, pp. 1586–1593, 2004.

[27] R. Millikan, E. Bishop, and A. T. Society, *Elements of Electricity: A Practical Discussion of the Fundamental Laws and Phenomena of Electricity and Their Practical Applications in the Business and Industrial World*. American Technical Society, 1917.

[28] C. Spearman, "The proof and measurement of association between two things," *The American Journal of Psychology*, vol. 15, no. 1, p. 72, 1904.

[29] F. Pedregosa, G. Varoquaux, A. Gramfort, V. Michel, B. Thirion, O. Grisel, M. Blondel, P. Prettenhofer, R. Weiss, V. Dubourg, J. Vanderplas, A. Passos, D. Cournapeau, M. Brucher, M. Perrot, and E. Duchesnay, "Scikit-learn: Machine Learning in Python ," *Journal of Machine Learning Research*, vol. 12, pp. 2825–2830, 2011.

[30] Python Software Foundation, "Python," 2019. [Online]. Available: https://www.python.org/

[31] F. Chollet *et al.*, "Keras," 2015. [Online]. Available: https://keras.io

[32] B. Xu, A. Oudalov, A. Ulbig, G. Andersson, and D. S. Kirschen, "Modeling of Lithium-Ion Battery Degradation for Cell Life Assessment," *IEEE Transactions on Smart Grid*, vol. 9, no. 2, pp. 1131–1140, 2018.

[33] M. Woody, M. Arbabzadeh, G. M. Lewis, G. A. Keoleian, and A. Stefanopoulou, "Strategies to limit degradation and maximize Li-ion battery service lifetime - Critical review and guidance for stakeholders," *Journal of Energy Storage*, vol. 28, p. 101231, 2020.

[34] V. Gold, Ed., *The IUPAC Compendium of Chemical Terminology*. International Union of Pure and Applied Chemistry (IUPAC), 2019.

[35] M. Berecibar, "Machine-learning techniques used to accurately predict battery life," *Nature*, vol. 568, pp. 325–326, 2019.

[36] K. Schwenk, M. Faix, R. Mikut, V. Hagenmeyer, and R. R. Appino, "On calendar-based scheduling for user-friendly charging of plug-in electric vehicles," in *2019 IEEE 2nd Connected and Automated Vehicles Symposium (CAVS)*. IEEE, 2019.

[37] A. Lew and H. Mauch, *Dynamic Programming - A computational tool*. Springer-Verlag GmbH, 2006.

[38] K. Schwenk, T. Harr, R. Großmann, R. R. Appino, V. Hagenmeyer, and R. Mikut, "Data-driven charging strategies for grid-beneficial, customer-oriented and battery-preserving electric mobility," in *Proceedings 29th Workshop Computational Intelligence, Dortmund, Germany*. KIT Scientific Publishing, 2019.

[39] Fraunhofer Institute for Solar Energy Systems ISE, "Energy-Charts," 2021. [Online]. Available: https://energy-charts.info/

[40] S. Meisenbacher, K. Schwenk, J. Galenzowski, S. Waczowicz, R. Mikut, and V. Hagenmeyer, "Smart Charging of Electric Vehicles with Cloud-based Optimization and a Lightweight User Interface: A Real-World Application in the Energy Lab 2.0: Poster," in *Proceedings of the Twelfth ACM International Conference on Future Energy Systems*, ser. e-Energy '21. Association for Computing Machinery, 2021.

[41] S. I. Sun, A. J. Chipperfield, M. Kiaee, and R. G. A. Wills, "Effects of market dynamics on the time-evolving price of second-life electric vehicle batteries," *Journal of Energy Storage*, vol. 19, pp. 41–51, 2018.

[42] G. Berckmans, M. Messagie, J. S. N. O. L. Vanhaverbeke, and J. V. Mierlo, "Cost Projection of State of the Art Lithium-Ion Batteries for Electric Vehicles up to 2030," *Energies*, vol. 10, no. 9, p. 1314, 2017.

[43] I.-Y. L. Hsieh, M. S. Pan, Y.-M. Chiang, and W. H. Green, "Learning only buys you so much: Practical limits on battery price reduction," *Applied Energy*, vol. 239, pp. 218–224, 2019.

[44] F. Ayadi, I. Colak, I. Garip, and H. I. Bulbul, "Impacts of Renewable Energy Resources in Smart Grid," in *2020 8th International Conference on Smart Grid (icSmartGrid)*. IEEE, 2020.

[45] M. Carrion, "Determination of the selling price offered by electricity suppliers to electric vehicle users," *IEEE Transactions on Smart Grid*, vol. 10, no. 6, pp. 6655–6666, 2019.

This work is licensed under a Creative Commons Attribution 4.0 License. For more information, see https://creativecommons.org/licenses/by/4.0/

This article has been accepted for publication in a future issue of this journal, but has not been fully edited. Content may change prior to final publication. Citation information: DOI 10.1109/TSG.2021.3099206, IEEE Transactions on Smart Grid

Karl Schwenk received the M.Sc. degree in mechanical engineering from the Karlsruhe Institute of Technology, Karlsruhe, Germany in 2018. He is currently pursuing his Ph.D. at the Institute for Automation and Applied Informatics with the Karlsruhe Institute of Technology in cooperation with Mercedes-Benz AG, Sindelfingen, Germany. His research topics comprise automated charging assistants for electric vehicles considering power supply, battery degradation and user constraints.

Stefan Meisenbacher received the B.Eng. in mechanical engineering from the Esslingen University of Applied Sciences, Esslingen, Germany in 2017, and the M.Sc. degree in mechanical engineering from the Karlsruhe Institute of Technology, Karlsruhe, Germany in 2020. He is currently pursuing a Ph.D. in the field of modeling, machine-learning based forecasting and model application surveillance at the Institute for Automation and Applied Informatics within the Karlsruhe Institute of Technology.

Benjamin Briegel received the Dipl.-Ing. degree in mechanical engineering from the University of Stuttgart, Stuttgart, Germany, in 2014. He is currently working as a development engineer in the area of eDrive innovations at Mercedes-Benz AG in Sindelfingen, Germany. His work topics include the development of digital services for electric vehicles with a focus on optimal charging.

Tim Harr received the Ph.D. degree in electrical engineering from the University of Ulm, Ulm, Germany, in 2007. He is currently working as a development engineer in the area of eDrive innovations at Mercedes-Benz AG in Sindelfingen, Germany. His work topics include the development of connected services to detect and predict the usage behavior of electric vehicles.

Veit Hagenmeyer received the Ph.D. degree from Université Paris XI, Paris, France in 2002. He is currently the Professor in energy informatics with the Faculty of Informatics, and the Director of the Institute for Automation and Applied Informatics with the Karlsruhe Institute of Technology, Karlsruhe, Germany. His research interests include modeling, optimization and control of sector-integrated energy systems, machine-learning based forecasting of uncertain demand and production in energy systems mainly driven by renewables, and integrated cyber-security of such systems.

Ralf Mikut received the Dipl.-Ing. degree in automatic control from the University of Technology, Dresden, Germany, in 1994, and the Ph.D. degree in mechanical engineering from the University of Karlsruhe, Karlsruhe, Germany, in 1999. Since 2011, he is Adjunct Professor at the Faculty of Mechanical Engineering and Head of the Research Group "Automated Image and Data Analysis" at the Institute for Automation and Applied Informatics of the Karlsruhe Institute of Technology (KIT), Germany. His current research interests include machine learning, image processing, life science applications and smart grids.

This work is licensed under a Creative Commons Attribution 4.0 License. For more information, see https://creativecommons.org/licenses/by/4.0/